



$\text{CdS}_x\text{Te}_{1-x}$ Alloying in CdS/CdTe Solar Cells

Preprint

Joel N. Duenow, Ramesh G. Dhere,
Helio R. Moutinho, Bobby To, Joel W. Pankow,
Darius Kuciauskas, and Timothy A. Gessert

*Presented at the 2011 Materials Research Society Spring Meeting
San Francisco, California
April 25–29, 2011*

NREL is a national laboratory of the U.S. Department of Energy, Office of Energy Efficiency & Renewable Energy, operated by the Alliance for Sustainable Energy, LLC.

Conference Paper
NREL/CP-5200-50156
May 2011

Contract No. DE-AC36-08GO28308

NOTICE

The submitted manuscript has been offered by an employee of the Alliance for Sustainable Energy, LLC (Alliance), a contractor of the US Government under Contract No. DE-AC36-08GO28308. Accordingly, the US Government and Alliance retain a nonexclusive royalty-free license to publish or reproduce the published form of this contribution, or allow others to do so, for US Government purposes.

This report was prepared as an account of work sponsored by an agency of the United States government. Neither the United States government nor any agency thereof, nor any of their employees, makes any warranty, express or implied, or assumes any legal liability or responsibility for the accuracy, completeness, or usefulness of any information, apparatus, product, or process disclosed, or represents that its use would not infringe privately owned rights. Reference herein to any specific commercial product, process, or service by trade name, trademark, manufacturer, or otherwise does not necessarily constitute or imply its endorsement, recommendation, or favoring by the United States government or any agency thereof. The views and opinions of authors expressed herein do not necessarily state or reflect those of the United States government or any agency thereof.

Available electronically at <http://www.osti.gov/bridge>

Available for a processing fee to U.S. Department of Energy and its contractors, in paper, from:

U.S. Department of Energy
Office of Scientific and Technical Information

P.O. Box 62
Oak Ridge, TN 37831-0062
phone: 865.576.8401
fax: 865.576.5728
email: <mailto:reports@adonis.osti.gov>

Available for sale to the public, in paper, from:

U.S. Department of Commerce
National Technical Information Service
5285 Port Royal Road
Springfield, VA 22161
phone: 800.553.6847
fax: 703.605.6900
email: orders@ntis.fedworld.gov
online ordering: <http://www.ntis.gov/help/ordermethods.aspx>

Cover Photos: (left to right) PIX 16416, PIX 17423, PIX 16560, PIX 17613, PIX 17436, PIX 17721



Printed on paper containing at least 50% wastepaper, including 10% post consumer waste.

CdS_xTe_{1-x} Alloying in CdS/CdTe Solar Cells

Joel N. Duenow, Ramesh G. Dhere, Helio R. Moutinho, Bobby To, Joel W. Pankow, Darius Kuciauskas, and Timothy A. Gessert
National Renewable Energy Laboratory, 1617 Cole Blvd., Golden, CO 80401

ABSTRACT

A CdS_xTe_{1-x} layer forms by interdiffusion of CdS and CdTe during the fabrication of thin-film CdTe photovoltaic (PV) devices. The CdS_xTe_{1-x} layer is thought to be important because it relieves strain at the CdS/CdTe interface that would otherwise exist due to the 10% lattice mismatch between these two materials. Our previous work [1] has indicated that the electrical junction is located in this interdiffused CdS_xTe_{1-x} region. Further understanding, however, is essential to predict the role of this CdS_xTe_{1-x} layer in the operation of CdS/CdTe devices. In this study, CdS_xTe_{1-x} alloy films were deposited by RF magnetron sputtering and co-evaporation from CdTe and CdS sources. Both radio-frequency-magnetron-sputtered and co-evaporated CdS_xTe_{1-x} films of lower S content ($x < 0.3$) have a cubic zincblende (ZB) structure akin to CdTe, while those of higher S content have a hexagonal wurtzite (WZ) structure like that of CdS. Films become less preferentially oriented as a result of a CdCl₂ heat treatment at ~400°C for 5 min. Films sputtered in a 1% O₂/Ar ambient are amorphous as deposited, but show CdTe ZB, CdS WZ, and CdTe oxide phases after a CdCl₂ heat treatment (HT). Films sputtered in O₂ partial pressure have a much wider bandgap (BG) than expected. This may be explained by nanocrystalline size effects seen previously [2] for sputtered oxygenated CdS (CdS:O) films.

INTRODUCTION

A CdS_xTe_{1-x} layer forms by interdiffusion of CdS and CdTe during the fabrication of thin-film CdTe PV devices in the standard superstrate configuration. High-temperature processing steps such as the close-spaced sublimation of CdTe and the post-deposition CdCl₂ HT contribute to formation of this alloy [1]. The CdS_xTe_{1-x} layer is thought to be important in fabricating high-performance CdTe devices because it relieves strain at the CdS/CdTe interface that would otherwise exist due to the large lattice mismatch (~10%) between these two materials. Our previous work indicated that the electrical junction is located in this interdiffused CdS_xTe_{1-x} region between a structurally compatible Te-rich n-type CdS_xTe_{1-x} alloy and p-type CdTe [1,3].

The CdS_xTe_{1-x} alloy has been found to follow Vegard's Law [4], such that lattice parameter values obtained from X-ray diffraction measurements can be used to calculate the mole fraction (x) for different phases of CdS_xTe_{1-x}. The BG of CdS_xTe_{1-x} has been described as a quadratic function of x [5], with values decreasing below the CdTe BG value of 1.5 eV, to as low as 1.41 eV at $x \sim 0.3$, before increasing at higher x values. The alloy system also exhibits a miscibility gap (two-phase region) in which both a CdTe-rich ZB phase and CdS-rich WZ phase may be present simultaneously at equilibrium. The composition of each phase in the two-phase region is the same as in the corresponding single-phase regions at the edges of the miscibility gap, with the relative quantity of each phase present varying with x [6]. Single-phase films, however, have been grown within the miscibility gap, implying non-equilibrium growth methods were used. The phases generally separated after a CdCl₂ HT [6-8]. We found similar behavior in this study.

Further understanding of $\text{CdS}_x\text{Te}_{1-x}$ alloys is essential to predict the role of the $\text{CdS}_x\text{Te}_{1-x}$ layer in the operation of CdS/CdTe devices. In this study, we investigate this alloy layer by depositing $\text{CdS}_x\text{Te}_{1-x}$ films using two methods.

EXPERIMENTAL DETAILS

We deposited $\text{CdS}_x\text{Te}_{1-x}$ films by radio frequency (RF) magnetron sputtering using targets of three compositions: 10/90, 25/75, and 60/40 wt.% CdS/CdTe. Films were deposited at room temperature (RT; no intentional heating) and at 300°C. Because little difference was seen between films grown at RT and at 300°C, only the 300°C results are presented here. In addition, two deposition ambients were used—100% Ar and 1% O_2/Ar . The ratio was measured using an ion gauge. Films were also deposited by co-evaporation from CdTe and CdS sources using Radak II effusion cells. The geometry of the co-evaporation system enabled us to obtain a range of compositions during a single deposition. The films were deposited onto three different substrates—Corning 7059 glass, Corning 7059 glass/450 nm $\text{SnO}_2/\text{F}/150$ nm SnO_2 , and Corning 7059 glass/ $\text{SnO}_2/\text{F}/\text{SnO}_2/125$ nm sputtered CdS:O—to be amenable to the different types of characterization performed on the films. Reflectance and transmittance measurements were performed using a Cary 6000i UV-Vis-NIR spectrophotometer. Electron probe microanalysis (EPMA) was performed using a beam energy of 5 kV to obtain film composition. X-ray diffraction (XRD; Rigaku Ultima IV) θ -2 θ measurements were performed using $\text{Cu K}\alpha$ radiation to examine the structure of the $\text{CdS}_x\text{Te}_{1-x}$ films. Electron backscatter diffraction (EBSD; FEI FEG SEM Nova 630 NanoSEM with an EDAX Pegasus/Hikari A40 EDS/EBSD system) measurements were performed to examine grain orientation and size for selected films.

RESULTS AND DISCUSSION

Composition of the ~150-nm-thick sputtered $\text{CdS}_x\text{Te}_{1-x}$ alloy films was measured using EPMA (Fig. 1, left panel). Films were grown in 100% Ar and 1% O_2/Ar both before and after a 5 min. vapor CdCl_2 HT at 400°C. Films grown from the 10/90 wt.% CdS/CdTe target show little compositional change between the different deposition ambients and after the CdCl_2 HT. Films

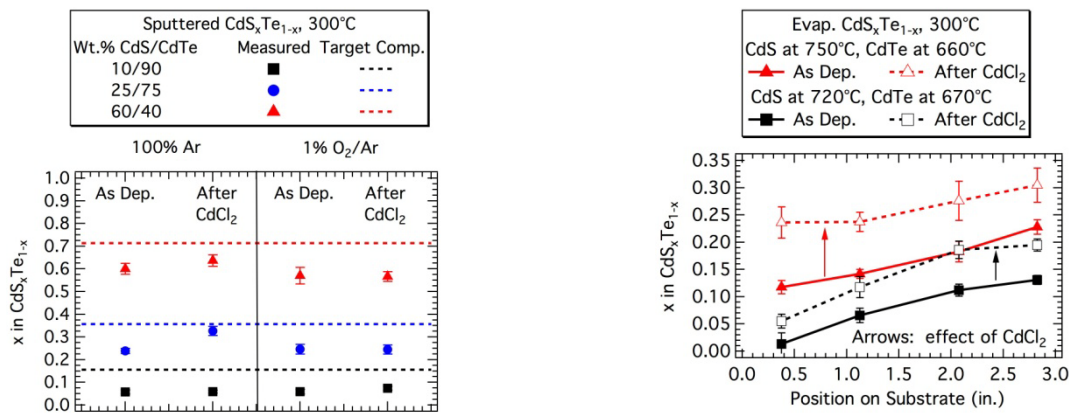


Fig. 1. Measured x values for sputtered (left) and evaporated (right) $\text{CdS}_x\text{Te}_{1-x}$ films from EPMA. Dashed lines in the left plot indicate the manufacturer’s stated target composition. Evaporated films were measured at four positions because of the inherent composition gradient across the substrate due to the deposition system geometry.

grown from the 25/75 and 60/40 wt.% CdS/CdTe targets in the 100% Ar ambient display a slight enrichment in S (or, equivalently, a loss of Te) after the CdCl₂ HT. All films appear S-deficient, however, compared to the manufacturer's stated target composition. This may be due to differences in sticking coefficient on the substrate of the S and Te species. Two ~300-nm-thick evaporated CdS_xTe_{1-x} films (Fig. 1, right panel) were deposited using different combinations of CdS and CdTe effusion cell temperatures. The as-deposited films (solid lines) show the expected gradient in x across the substrate. The evaporated films also show a significant relative enhancement in S (or loss of Te) after the CdCl₂ HT.

CdS_xTe_{1-x} alloy film structure was investigated using XRD. θ -2 θ scans of films grown from the 10/90 wt.% CdS/CdTe target in the 100% Ar and 1% O₂/Ar ambients both before and after a CdCl₂ HT are shown in Fig. 2. Films examined using XRD were deposited on Corning 7059 glass/450 nm SnO₂:F/150 nm SnO₂/125 nm sputtered CdS:O substrates similar to those used for CdTe PV devices. Tetragonal SnO₂, cubic ZB CdTe, and hexagonal WZ CdS peaks are indicated. The as-deposited film grown in 100% Ar shows one prominent peak, CdTe ZB (111). Other peaks in this spectrum are due to the SnO₂ films on the substrate. After a CdCl₂ HT is performed on this film, the CdTe ZB (111) peak decreases in intensity, while small CdTe ZB (220) and (311) peaks, and CdS WZ (100), (002), and (101) peaks, appear. This behavior indicates a decrease in preferential orientation after the CdCl₂ HT. The film grown in 1% O₂/Ar is amorphous as deposited. After the CdCl₂ HT, however, many CdTe ZB and CdS WZ phases appear, in addition to prominent CdTe oxide phases (e.g. CdTeO₃, CdTe₂O₅). Further work is required to identify which oxide phases are dominant. A summary of XRD results for the sputtered films is shown in Table 1. Films grown in 100% Ar from the 60/40 wt.% CdS/CdTe target contain only CdS WZ phases, both before and after the CdCl₂ HT, while films of higher CdTe content in this ambient show both CdTe ZB and CdS WZ phases. All films grown in 1% O₂/Ar are amorphous as deposited. The CdTe oxide peaks observed after the CdCl₂ HT are much less intense for the 25/75 and 60/40 wt.% CdS/CdTe films than for the 10/90 wt.% film.

XRD measurements were also performed on evaporated CdS_xTe_{1-x} alloy films both before and after a CdCl₂ HT at 390°C. Measurements were performed at several points on the film because of the composition gradient. The CdTe ZB (111) peak was observed to shift to an intermediate position between it and the adjacent CdS WZ (100) peak as the S content increased.

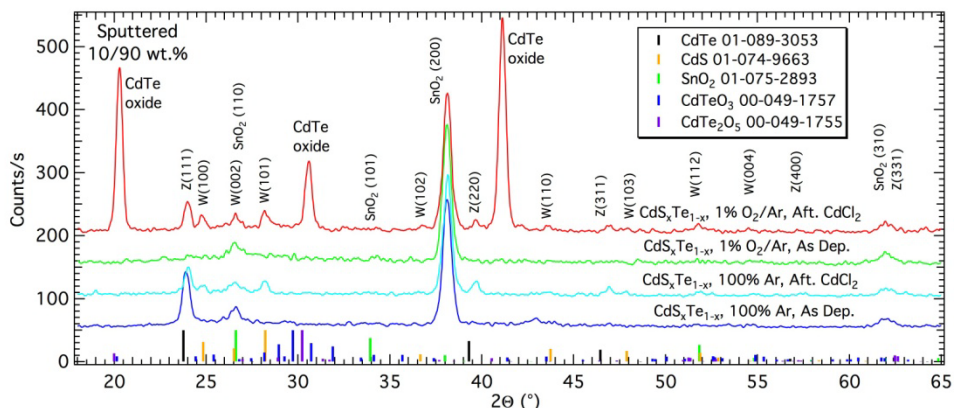


Fig. 2. XRD scans for sputtered CdS_xTe_{1-x} films grown from the 10/90 wt.% CdS/CdTe target. Growth ambient and post-deposition treatment are shown on the plot. Peak positions from the powder diffraction files corresponding to these materials are shown at the bottom (with corresponding file numbers shown in the upper right).

Table 1. Phases present in sputtered $\text{CdS}_x\text{Te}_{1-x}$ films grown in 100% Ar and 1% O_2/Ar before and after a CdCl_2 HT.

Wt.% CdS/ CdTe	100% Ar		1% O_2/Ar	
	As Dep.	Aft. CdCl_2	As Dep.	Aft. CdCl_2
10/90	CdTe ZB	CdTe ZB CdS WZ	Amorphous	CdTe ZB CdS WZ Strong Oxide Phases
25/75	CdTe ZB Minor CdS WZ	CdTe ZB CdS WZ	Amorphous	CdTe ZB CdS WZ Oxide Phases
60/40	CdS WZ	CdS WZ	Amorphous	CdS WZ Oxide Phases

After the CdCl_2 HT, the CdTe ZB (111) peak shifts toward its expected position, while other CdTe ZB and CdS WZ phases appear, indicating a decrease in film preferential orientation. These data are summarized in Table 2. The separation of the CdTe ZB (111) and CdS WZ (100) peaks suggests that phase separation occurs as a result of the CdCl_2 HT.

Analysis was performed to extract the lattice constants and mole fraction of the CdTe ZB phase from the XRD data. The lattice constant a_{Cubic} was determined using

$a_{\text{Cubic}} = d\sqrt{h^2 + k^2 + l^2}$, where $d = \lambda_a / (2 \sin \theta)$ is calculated from the measured 2θ peak position, $\lambda_a = 1.540562 \text{ \AA}$ is the wavelength of the Cu K_α radiation, and h , k , and l are the Miller indices for the diffraction peak. When multiple CdTe ZB peaks were present, the a_{Cubic} values were plotted as a function of the Nelson-Riley-Sinclair-Taylor (NRST) function [6],

$$NRST = \frac{1}{2} \left(\frac{\cos^2 \theta}{\sin \theta} + \frac{\cos^2 \theta}{\theta} \right).$$

Fitting a line to these points enabled a lattice constant of greater precision to be found by extrapolating to normal incidence at $NRST=0$ [6]. Vegard's law, which applies to the CdTe-CdS alloy system [4], was then used to determine the mole fraction, x , for the cubic ZB phase:

$$x = \frac{a_{\text{CdS}_x\text{Te}_{1-x}(\text{Cubic})} - a_{\text{CdTe}}}{a_{\text{CdS}} - a_{\text{CdTe}}}.$$

For cubic phases, $a_{\text{CdTe}} = 6.481 \text{ \AA}$ and $a_{\text{CdS}} = 5.818 \text{ \AA}$.

Fig. 3 compares the x values obtained from EPMA and XRD for $\text{CdS}_x\text{Te}_{1-x}$ alloy films sputtered in 100% Ar and subjected to a CdCl_2 HT. EPMA values measure the composition of the whole film. At higher S contents, EPMA values strongly exceed those obtained using the XRD analysis of the CdTe cubic ZB peaks, which measures the composition of the ZB phase only. The difference indicates that the film composition is within the CdS/CdTe miscibility gap for films of the higher two S contents. The miscibility gap was measured to lie between $x=0.058$ and $x=0.97$ [7] at temperatures of 415°C . Mole fraction values measured by XRD for the Te-rich cubic ZB phase in this study are consistent with the $x=0.058$ observed by Jensen *et al.* [7]. Similar x values were observed for the evaporated films also (not shown).

To obtain information about grain orientation and size in these films, EBSD measurements were performed (Fig. 4) on $\text{CdS}_x\text{Te}_{1-x}$ alloy films grown on Corning 7059/ $\text{SnO}_2:\text{F}/\text{SnO}_2/\text{CdS}:\text{O}$ substrates. One sputtered and one evaporated film were measured after a CdCl_2 HT and a 2 s 0.5%-concentrated bromine-methanol etch. Grains of both films are randomly oriented, indicated by the different colors of each grain. Pole figures (not shown) confirm this random orientation. The grain size of the sputtered film is 360 nm, while that of the evaporated film is 240 nm. This

Table 2. Phases present in evaporated $\text{CdS}_x\text{Te}_{1-x}$ films before and after a CdCl_2 HT.

CdS Content	As Dep.	Aft. CdCl_2
Lower ($x = 0.01$ to 0.12 as dep.)	CdTe ZB (111)	CdTe ZB Minor CdS WZ
Higher ($x = 0.12$ to 0.23 as dep.)	CdTe ZB (111), shifted toward CdS WZ (100) at high S	CdTe ZB CdS WZ

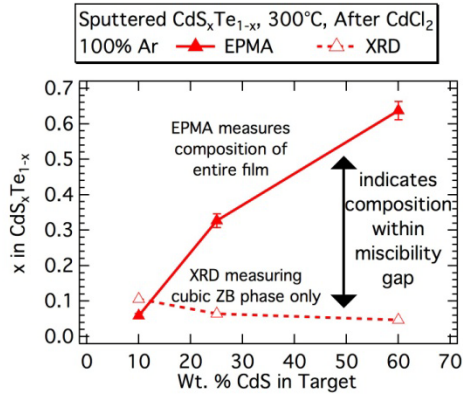


Fig. 3. Mole fraction (x) obtained from EPMA and XRD measurements for sputtered $\text{CdS}_x\text{Te}_{1-x}$ films.

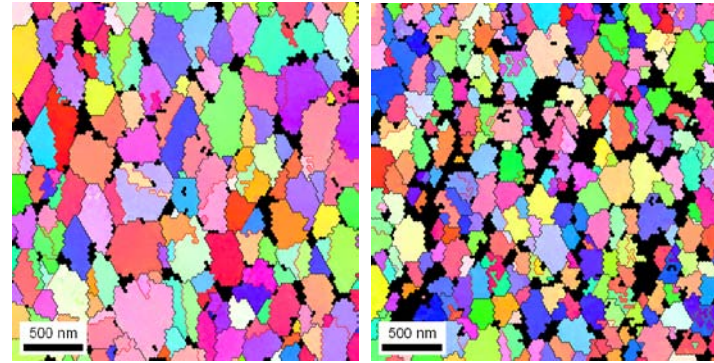


Fig. 4. EBSD images for a sputtered film (left; $x=0.059$, grain size 360 nm) and an evaporated film (right; $x=0.28$, grain size 240 nm). Black lines indicate grain boundaries; red lines indicate $\Sigma 3$ twin boundaries. Both films were imaged after a CdCl_2 HT.

difference may be due to the greater adatom surface energy of the sputtering process. The CdCl_2 HT temperature for the sputtered film was also 10°C higher (400°C vs. 390°C), which may have contributed to increased recrystallization.

The BG of sputtered and evaporated $\text{CdS}_x\text{Te}_{1-x}$ films was calculated by measuring the

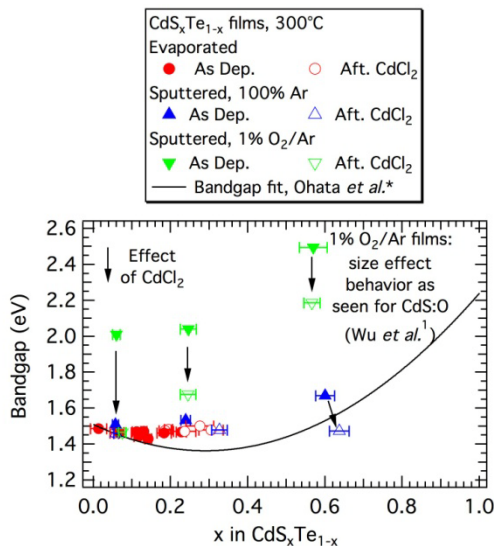


Fig. 5. Bandgap vs. mole fraction (x) for sputtered and evaporated $\text{CdS}_x\text{Te}_{1-x}$ films. The black curve was determined by Ohata *et al.* [5] by fitting experimental data.

reflectance and transmittance, calculating the absorption coefficient (α) [9], and plotting $(\alpha h\nu)^2$ vs. $h\nu$, where $h\nu$ is the photon energy. The evaporated films appear to have similar BG values (Fig. 5), indicating that these films have phase-separated due to the miscibility gap. The sputtered films deposited in the 100% Ar ambient also appear to have values near the 1.5 eV BG of CdTe. An interesting phenomenon was observed for the films deposited in the 1% O_2/Ar ambient. As deposited, these films had BG values much higher than expected. In fact, the 60/40 wt.% CdS/CdTe film had a BG value higher than that of CdS itself. We suspect this behavior is similar to that observed for CdS:O by Wu *et al.* [2], in which CdS films were sputtered in O_2 partial pressure. In that study, amorphous CdS:O films with BGs of up to 3.1 eV were deposited. The increase in BG was attributed to nanocrystalline quantum size effect

behavior. We believe a similar effect is occurring in $\text{CdS}_x\text{Te}_{1-x}$ films deposited in O_2 partial pressure. After a CdCl_2 HT, the low-S film decreases to a BG near that of CdTe, while the higher-S films decrease in BG substantially, but not to the expected levels. This decrease is consistent with partial grain recrystallization and growth taking place as a result of the HT, though it seems to be incomplete.

CONCLUSIONS

$\text{CdS}_x\text{Te}_{1-x}$ alloy films were deposited by RF magnetron sputtering and co-evaporation. As-deposited sputtered films grown in 100% Ar from targets containing 10/90 and 25/75 wt.% CdS/CdTe have a cubic CdTe ZB structure, while those grown from a target of 60/40 wt.% CdS/CdTe have a hexagonal CdS WZ structure. Films become less preferentially oriented as a result of a vapor CdCl_2 HT at 400°C for 5 min. Films sputtered in a 1% O_2/Ar ambient are amorphous as deposited, but show CdTe ZB, CdS WZ, and CdTe oxide phases after a CdCl_2 HT. Evaporated films primarily consist of the CdTe ZB phase as deposited, but the CdTe ZB (111) peak is shifted significantly toward the adjacent CdS WZ (100) peak for films of higher S content. These two peaks become distinct after a CdCl_2 HT, indicating phase separation has occurred. Both sputtered and evaporated films have randomly oriented grains after a CdCl_2 HT. The grain size of the sputtered film is larger than that of the evaporated film (360 vs. 240 nm). $\text{CdS}_x\text{Te}_{1-x}$ alloy films sputtered in 1% O_2/Ar are amorphous as deposited and have a much higher bandgap than expected. This may be explained by nanocrystalline size effects seen previously [2] for CdS:O films.

Future work will include additional EBSD measurements to identify $\text{CdS}_x\text{Te}_{1-x}$ phases and their intermixing both before and after a CdCl_2 HT. Auger electron spectroscopy and X-ray photoelectron spectroscopy will be used to examine the CdTe oxides that result from the CdCl_2 HT of films grown in 1% O_2/Ar . In future PV device work, we plan to replicate the existing superstrate device structure using directly deposited $\text{CdS}_x\text{Te}_{1-x}$ layers in PV devices. We also expect to design and deposit new superstrate and substrate PV device structures utilizing these directly deposited layers.

ACKNOWLEDGEMENTS

This work was supported by the U.S. Department of Energy under Contract No. DE-AC36-08GO28308 with the National Renewable Energy Laboratory.

REFERENCES

1. R. G. Dhere, Y. Zhang, M. J. Romero, S. E. Asher, M. Young, B. To, R. Noufi, and T. A. Gessert, *Proc. of the 33rd Photovoltaic Specialists Conference* (IEEE, San Diego, CA, 2008).
2. X. Wu, Y. Yan, R. G. Dhere, Y. Zhang, J. Zhou, C. Perkins, and B. To, *phys. stat. sol. (c)* **1**, 1062-1066 (2004).
3. R. G. Dhere, Ph.D. Thesis, University of Colorado, 1997.
4. K. Ohata, J. Saraie, and T. Tanaka, *Japan. J. Appl. Phys.* **12**, 1198-1204 (1973).
5. K. Ohata, J. Saraie, and T. Tanaka, *Japan. J. Appl. Phys.* **12**, 1641-1642 (1973).
6. D. G. Jensen, Ph.D. Thesis, Stanford University, 1997.
7. D. G. Jensen, B. E. McCandless, and R. W. Birkmire, *Proc. of of the 25th Photovoltaic Specialists Conference* (IEEE, Washington, D.C., 1996).
8. B. E. McCandless, G. M. Hanket, D. G. Jensen, and R. W. Birkmire, *J. Vac. Sci. Technol. A* **20**, 1462-1467 (2002).
9. J. I. Pankove, *Optical Processes in Semiconductors* (Dover Publications, Inc., New York, NY, 1971).